



## Shear Connection Behaviour and Performance of Steel-Concrete Composite Beams under Seismic and Load Conditions: A Finite Element Analysis



Isametova Madina Esdauletova<sup>1</sup>, Yan Cao<sup>2</sup>, Miloš Milovančević<sup>3\*</sup>

<sup>1</sup> School of Transport Engineering and Logistics, Satbayev University, 050000 Almaty, Kazakhstan

<sup>2</sup> School of Mechatronic Engineering, Xi'an Technological University, 710021 Xi'an, China

<sup>3</sup> Faculty of Mechanical Engineering, Univesity of Niš, 18000 Niš, Serbia

\* Correspondence: Miloš Milovančević (milos.milovancevic@masfak.ni.ac.rs)

Received: 10-05-2024

Revised: 11-17-2024

Accepted: 11-26-2024

**Citation:** I. M. Esdauletova, Y. Cao, and M. Milovančević, "Shear connection behaviour and performance of steel-concrete composite beams under seismic and load conditions: A finite element analysis," *J. Eng. Manag. Syst. Eng.*, vol. 3, no. 4, pp. 210–225, 2024. <https://doi.org/10.56578/jemse030403>.



© 2024 by the author(s). Published by Acadlore Publishing Services Limited, Hong Kong. This article is available for free download and can be reused and cited, provided that the original published version is credited, under the CC BY 4.0 license.

**Abstract:** The shear connection behaviour of steel-concrete composite beams is primarily governed by the strength of the connectors and concrete. Modern seismic evaluations and vibrational analyses of composite beams, particularly concerning their load-slip characteristics and shear strength, predominantly rely on push-out test data. In this study, the Finite Element Method (FEM) has been employed to simulate and analyse the shear, bending, and deflection responses of composite beams subjected to various load conditions, in accordance with Eurocode 4 standards. Failure modes, ultimate loads, and sectional capacities were examined in detail. The results indicate that increased strength of both steel and concrete significantly enhances the beam's capacity in bending. Specifically, flexural and compressive resistance showed marginal improvements of 3.2%, 3.1%, and 3.0%, respectively, as concrete strength increased from 25 N/mm<sup>2</sup> to 30, 35, and 40 N/mm<sup>2</sup>, while steel strength increased by 27% and 21%, with yield strengths of 275 N/mm<sup>2</sup>, 355 N/mm<sup>2</sup>, and 460 N/mm<sup>2</sup>, respectively. Under seismic loading, however, the ultimate flexural load capacity exhibited a reduction with a fixed beam span, irrespective of steel strength. The shear capacity remained constant across varying beam lengths but demonstrated significant improvements with increased steel yield strength, with enhancements of 29% and 67% as steel yield strength increased from 275 N/mm<sup>2</sup> to 355 N/mm<sup>2</sup> and 460 N/mm<sup>2</sup>, respectively. A detailed vibration analysis was also conducted to investigate the dynamic behaviour of these composite beams under seismic conditions. These findings underscore the critical influence of material strengths and loading conditions on the performance of steel-concrete composite beams, particularly in seismic scenarios, providing valuable insights for the design and assessment of such structures in seismic-prone regions.

**Keywords:** Cold-formed steel; Shear connector; Composite slab; Composite beam; Bending resistance

### 1 Introduction

Shear connection effectiveness depends on concrete and connection toughness. Experimental push-off testing of load-slip and shear connector capabilities reveals that connector strength and solidity affect shear connection behavior. Full-scale push-off testing is costly and time-consuming; therefore, analytical techniques that predict nonlinear responses and push-off capabilities are replacing most tests following chosen experimental results. Computer simulations are typically used instead of statistical modeling of push-off tests due to the complexity of three-dimensional stress states and shear connector-concrete interfaces. ABAQUS (2001) was used to develop a three-dimensional finite element model to simulate the behavior of cost-effective composite beams with heading shear angle connections. For shear connection failure mechanisms, ultimate strength, and load-slip characteristics, recent computer models simulated push-off test techniques with linear and nonlinear behaviors. Current FE model findings were compared to push-off tests and codes of practice values. Concrete strength and angle diameters were tested parametrically. The composite nature of shear connections depends on interface shearing capability and slip. A thorough composite beam test is best for simulating load-slip curves; however, a reduced push-off test is sometimes utilized. The push-out specimen, a short steel beam linked by shear connections to two small concrete plates (Figure 1), was placed immediately on the reaction floor and loaded at the higher end. Slip measurements between

steel and concrete slabs were taken at incremental load or displacement levels, with the average slip per connection load. This specimen resembles CP 117 [1].

Standard push-off specimens in efficient simulations assume a single angle per flange and homogenous load distribution from steel beam to connection. Modifying the finite element mesh while preserving concrete dimensions allowed the modeling of varied angle diameters, demonstrating that shear capacity can be estimated regardless of connection amount. The push-off specimen in Figure 1 has two concrete slabs on the flanges of a 254'3254 UC 73 steel beam. Each slab is 619 mm long, 469 mm wide, and 150 mm thick, with a 19 mm diameter and 100 mm height angle on each flange. In the load direction, the connection to the concrete edge is 200 mm for beams up to 50 mm adjacent to P117 (Figure 2). Transversely, the slab length (619 mm) meets EC4 [2]. Testing followed EC4, utilizing effective computer models and applying 20 kN increments up to 40% of the estimated failure load for 25 cycles. Slip measurements at each increment showed load-slip behavior unaffected by early cycles [3].

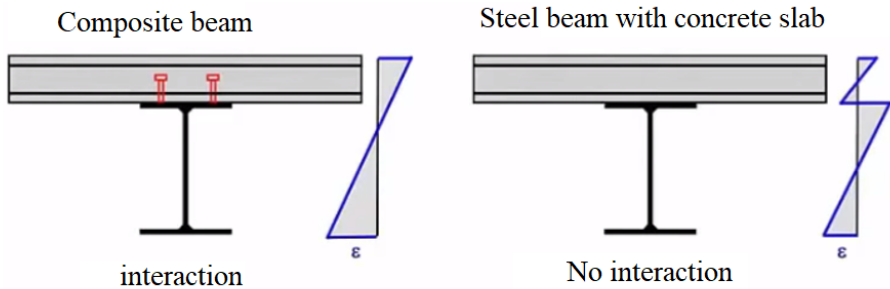


**Figure 1.** Composite beam (left) and steel beam with concrete slab (right)

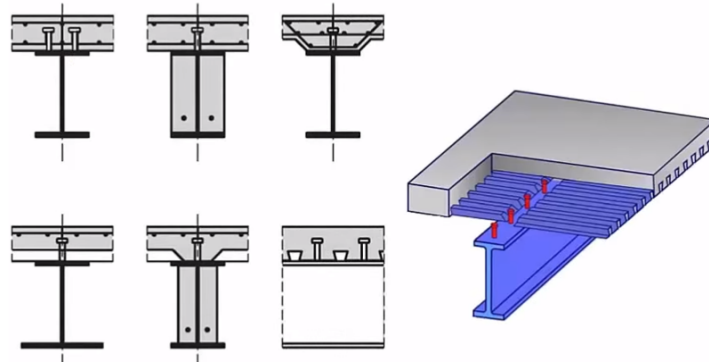


**Figure 2.** Composite beam cross sections

### 1.1 Ultimate Strength of Headed Shear Angle Connectors

BS 5950, AISC (1999), and EC4 set solid concrete plate shear angles [4]. Tabulated BS 5950 solid concrete slab-headed angle connection strength. In Table 1, Menzies (1971)'s regression research of regular push-off concrete cube strength and weight testing showed this linear relationship. AISC regulates nominal shear.

$$Q_n = 0.5A_{sc}\sqrt{f_c'E_c} < A_{sc}F_u \quad (1)$$

EC4 uses the following formulae to calculate ultimate angle connection resistance,  $P_R$ :

$$P_R = 0.29\alpha d^2 \sqrt{f_{ck}E_c} \quad (2)$$

And

$$P_R = 0.8f_u \frac{\pi d^2}{4} \quad (3)$$

Eq. (2) depicts concrete failure surrounding the connection, while Eq. (3) reveals shear connector failure (Figure 3).

**Table 1.** Specimen details

Specimen	Slab	CFS Channels (mm)	Shear Connector Size	Reinforcement	Reinforcement Ratio $\rho$
	Type of Slab	h b c	t	(mm)	(mm)
CBS1-CS-250-12-SC75	Composite slab	250 75 20	2.4	Ø12	C-75-45-15
CBS2-CS -150-12-R16	Composite slab	150 65 15	2.4	Ø12	Ø16
CBS3-CS -250-16-SC75	Composite slab	250 75 20	2.4	Ø16	C-75-45-15
CBS4-CS -150-16-R16	Composite slab	150 65 15	2.4	Ø16	Ø16
CBS5-CS -250-12-R20	Composite slab	250 75 20	2.4	Ø12	Ø20
CBS6-SS -250-12-SC75	Solid slab	250 75 20	2.4	Ø12	C-75-45-15
CBS7-SS -150-12-R16	Solid slab	150 65 15	2.4	Ø12	Ø16

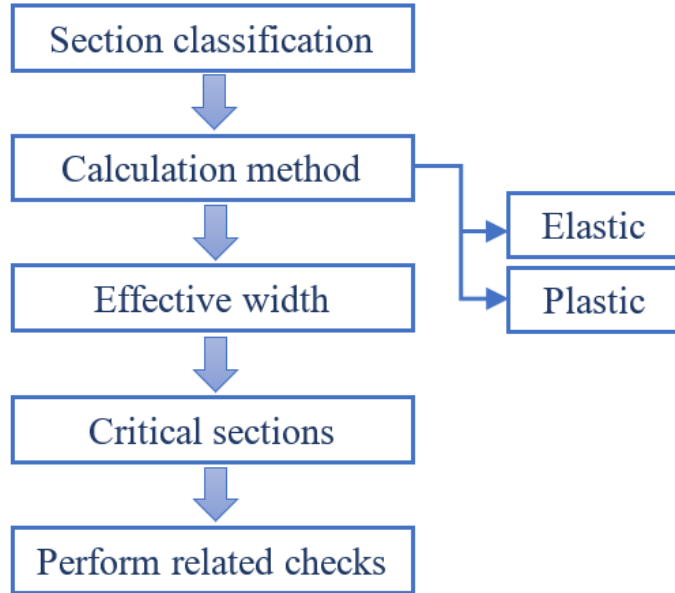


**Figure 3.** Composite beam design process

## 1.2 Material Model of Headed Shear Angle

The shear angle material is crucial to describing the steel-concrete shear connection because the area surrounding the angle suffers strong and dynamic stress. Shear connections at the steel-concrete interface transmit shearing forces. Three coupons were made from headed angles to test the angle material's mechanical qualities. A total trial rate of 470.8 N/mm<sup>2</sup> was 3. This average represents the maximum yield tension,  $f - ys$ , in angle material modeling. Figure 4 shows the header bolt stress-strain curve with the derived bilinear model. Young's modulus ( $E - s$ ) and yield strength ( $f - ys$ ) were used to describe an angular material as a linear elastic substrate. A building measure or bridge strengthened with steel beams is called an economic composite beam [5] if the two components are joined to work as a single unit. Characterising steel beams as concrete beams is cheaper, particularly on fire-prone bridges and multi-story car parks [6]. Till the 1950s, steel beams supported the maximum weight of concrete slabs and their loads. Shear connections were employed to link the slab to the beam. Composite beams are commonly bent by components. In a non-composite segment, steel beams support a concrete platform, making shear transfer impossible [7]. Shear connections between the concrete slab and steel beam prevent longitudinal slip at the component contact, improving structural resistance and stiffness and enabling operational synergy [8–10]. The angles prevent slippage and transmit shear load between the beams and slab. This increases beam strength and stiffness, reducing steel beam weight and depth [11]. Composite beams have a steel web and a concrete slab like T-beams [3, 12–14]. T-beams are flanged. The composite procedure may be completed by welding shear angles to the steel beam tops and embedding them in the concrete during casting (Figure 4). Comprehensive theoretical and scientific research has led to the increased usage of composite beams in residential and bridge building. Modern architecture requires aesthetic, economic, and mechanical construction measurement criteria. Using steel-concrete composites in construction offers a novel solution [8]. Concrete excels in compression but has inferior tensile strength compared to steel. Advantages include optimum concrete compression within the sheet and maximum structural strain on the steel beam [3]. Concrete, one of the most widely utilised human-made materials in civil engineering, is essential. Materials will come from EN 1993-1-1 for steel and EN 1992-1-1 for concrete [2, 7].

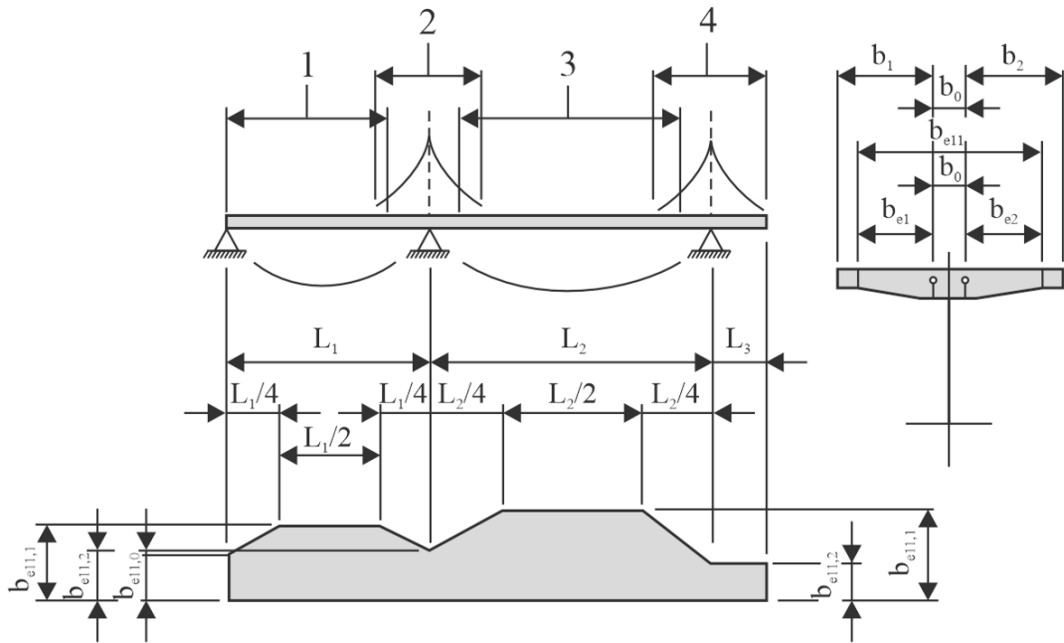
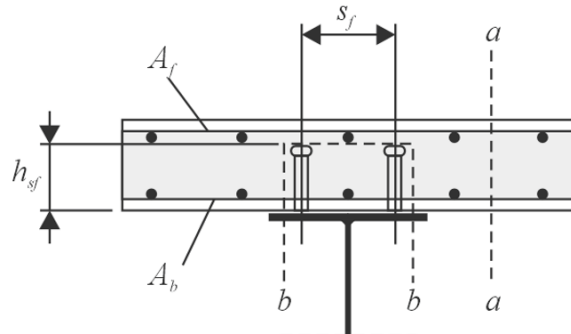


**Figure 4.** Effective width

### 1.3 Material Modeling of Steel Beam

This analysis employs the bilinear curve from Figure 5 to simulate the steel beam with a yield stress of 275 N/mm<sup>2</sup>. Computer modeling shows that the steel beam has no effect on push-off tests. It transfers applied force to connections, angling the load-slip characteristic at a concrete-steel contact.



$$\frac{A_{sf}f_{yd}}{s_f} \geq v_{Ed} \frac{h_f}{\cot \theta_f}$$

**Figure 5.** Left: Headed angle connection resistance, right: longitudinal shear

## 2 Methodology

The composite beam was modeled and assessed in ConSteel11 using finite elements. First, define the beam's cross-section. Composite beams with solid concrete slabs and profiled steel sheets are available. Moment redistribution using hard plastic or elastic principles is defined by the segment class. In the second step, a concrete slab composite with a stainless-steel beam is evaluated for its effective width using numerous methods, as illustrated in Figure 6. After identifying the important components, efficient computer simulations are used to test them. In addition to concrete fracture, economic composite beams must identify and evaluate cross sections with maximum bending moment, concentrated loads or responses, and rapid cross-section changes. Ultimate limit states and moment resistance are economic composite beam metrics for ultimate and serviceability limit states.



**Figure 6.** Angle welding

## 2.1 Top Limit States

1. Critical cross-section moment resistance.
2. Vertical shear resistance.
3. Longitudinal shear connector resistance.

## 2.2 Moment Resistance

The final composite section potential is independent of supported or unsupported construction. Plastic-neutral axis location determines composite section capacity. There are 3 outcomes [11, 15], plastic neutral axis in concrete, steel, and web flanges.

$X$  = Depth of neutral axis.

$H_t$  = Depth of concrete slab.

$H_g$  = Depth of centre of steel section from top of steel flange.

For balance, concrete and steel must have equal stress.

$$N_{cf} = \frac{A_a F_y}{y_a} = b_{eff} \frac{0.85 F_{ck}}{y_c} \quad (4)$$

If  $X \leq h_c$ , neutral axis in concrete slab, top flange moment, plastic moment resistance,

$$M_{PL,RD} = \frac{A_a F_y}{y_a} \left( h_g + h_t - \frac{x}{2} \right) \quad (5)$$

## 2.3 Moment Resistance

Composite beam shear resistance resembles steel beams. Concrete slab shear resistance is without impact (Figure 7).  $A_v = I_s$  = the shear area (the area of the beam web).

Figure 8 below shows the shear area of I section.



**Figure 7.** Angle welding on steel element

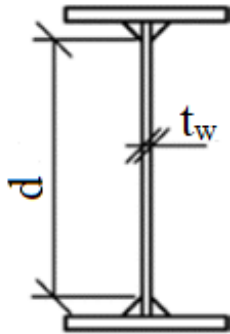


**Figure 8.** Shear area of shear

## 2.4 Resistance of Shear Connectors

Shear connections carry longitudinal shear from the concrete slab to the steel beam, which must resist shearing (Figure 9). Euro Code 4 shear capacity head angles are provided in Eq. (6).

$$P_{Rd} = \frac{0.8F_u\pi d^2/4}{yv} \quad (6)$$

$yv$  = Partial safety factor for the shear angle = 1.25

$d$  = shank diameter of the angle



**Figure 9.** Angle welding on steel element (Engine tips)

## 2.5 Deflection

Deflection elastically affects segment component modulus and moment of inertia. With the right modular ratio, the composite piece becomes a steel segment. Deflection calculation uses the uncracked portion's moment of inertia. Serviceability tests commonly utilise unfactored loads. No tension limits in research [15]. Composite beam deflectors are assessed like steel beams, employing a composite section for gross uncracked inertia.

$$\delta_{allow} = \frac{L}{360} \quad (7)$$

Uniformly distributed load simply supported by a beam, the deflection is:

$$\delta_{allow} = \frac{5W_qL^4}{364EI_g} \quad (8)$$

$W_q$  = imposed uniformly distributed load only;

$E = 205\text{KN/mm}^2$  is the elastic modulus of steel;

$I_g$  = the gross uncracked moment of inertia of composite section by Eq. (8):

$$I_g = I_a + \frac{Ab_{eff}h_t(h_a + h_t)^2}{4(Am + b_{eff}h_t)} \quad (9)$$

## 2.6 Loading

Considering the direct static loading based on Eurocode 1 (EC 1), the load  $W$  is given by Eq. (9):

$$W = y_G G_K + y_k Q_k \quad (10)$$

$y_G, y_k$  = partial safety factors for actions;

$G_K$  = the permanent action or self-weight;

$Q_K$  = the variable action based on type and function of the structure.

Its values depend on whether the behavior is unfavorable or beneficial for the result considered (Figure 10).

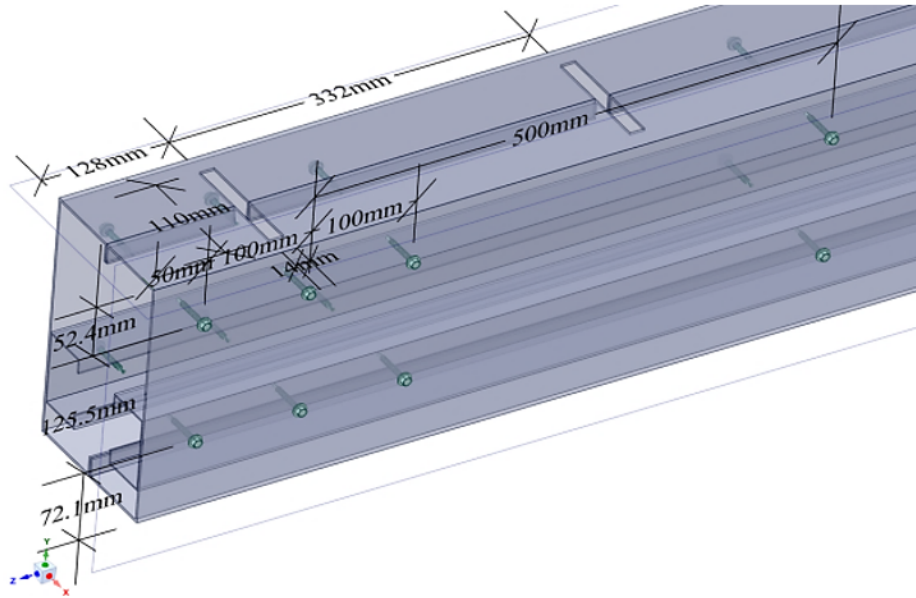


**Figure 10.** CFS built-up box section beams used in this research

## 2.7 Monotonic Behavior of Headed Angles Subjected to Shear Forces

A comprehensive set of static stress tests for headed steel anchors is listed in research [16], as is the case in studies [7, 10, 16]. Headed steel anchors were subjected to 391 tests to determine their repeating function. Failure of the steel, weld, or concrete around the headed angle might cause composite headed angle anchors to shatter. There were 114 concrete failures and 202 steel failures out of 391 headed steel angle tests. Additional failures were not documented or categorised as mixed by the author. There were 286 trials that utilised regular concrete and 125 that employed lightweight concrete in this set of results. Here are the experiment diagrams: Table 2. There are typically three kinds of push-off tests. The second kind of checked steel anchor may be laid horizontally under certain circumstances [13, 16]. For the third version, there are infill walls to think about (e.g., [13]). Pryout or steel failure in the push-off test may be simulated by an excellent computer model of the anchor between steel and concrete in composites. The AISC, EC-4 (2004), PCI 6th Edition, and ACI 318-08 tests were used. The strength of the heading angle is estimated by all four models for steel shank failure using a generic form of  $\phi_v C_v A_S n$ .

$A_S$  = cross sectional area of the headed angle;

$n$  = number of angles;

$\phi_v$  = resistance factor;

$C_v$  = a reduction factor of the strength;

$F_u$  = specified (nominal) minimum tensile strength of the headed angle anchor.

**Table 2.** Properties of the hardened concrete

Properties	C1	C2	C3	Average
Cube Compressive Strength $f_{cu}$ (N/mm <sup>2</sup> )	60.7	56.9	63.9	60.5
Cylinder Compressive Strength $f_{cd}$ (N/mm <sup>2</sup> )	48.6	45.5	51.2	48.4
Modulus of Elasticity $E_c$ (N/mm <sup>2</sup> )	37797.6	37072.1	38389.7	37753.1

Table 3 displays the coefficient values for all three standards. The nominal strength of a certain heading angle anchor, as determined by ACI 318-08 and PCI 6th, in the event of concrete failures, may be expressed as  $\phi_v C_v A_S n$ . The 5% fractile is the basis for these formulations; that is, they are built in a manner that occurs 90% of the time over the observed limit value for the condition of an individual anchor [16, 17]. Breakout and prout are two possible ways that concrete might fail in a composite design, as stated in ACI 318-08. The absence of unrestricted edge control causes a breakout. Under these conditions, the anchor is encased in a solid volume formed by faulty planes, which separates it from the component. A concrete spall configured perpendicular to the applied shear stress causes prout failure in the vicinity of the anchor. Since most composite components do not have proper front-edge or side-edge break-out failure planes, especially when normal reinforcing features are utilised, break-out failure in composite structures is not regarded as a significant limiting condition in this research. Additionally, break-out failure is rare in composite structures. Based on their research, Abdullah et al. [4] concluded that prout is the concrete failure mechanism seen in composite structures (or "in the region" in PCI 6th Edition terminology), as described by ACI 318-08. One way to estimate the prout failure ( $V_{cp}$ ) according to ACI 318-08 is to take the strain capacity ( $N_b$ ) of the concrete's breakout strength. But if the  $h_{ef}/d$  ratio is less than 4.5, there is a clear way to determine the prout failure in the sixth edition of PCI. Any steel shank with a  $h_{ef}/d$  ratio higher than 4.5 is prone to failure. For a quick review of the formula used to calculate the prout loss in ACI 318-08 and PCI 6 Edition, see Table 3. The shear strength calculation formula is provided by AISC for composite products other than composite beams. The 48 test results were derived from their study, which included adjusting several models using efficient computer modeling. The formula was based on the work of Dizaji and Dizaji [15] on headed steel anchors in composite beams. The resilience of headed steel anchors often does not have its own AISC resistance factor since its stability is now considered as part of the design of composite portions, such as composite columns, to avoid premature collapse. As an alternative, Euro-code 4 recommends using the same shear strength calculation method for composite components. In contrast to study [18], this method affects partial protection factors (Table 3), leading to more cautious outcomes (Figure 11).

**Table 3.** Properties of the hardened concrete

Material	Diameter/Thickness	Yield Stress $f_y$	Ultimate Stress $f_u$	Elastic Modulus $E_s$	$f_u/f_y$
	mm	( N/mm <sup>2</sup> )	( N/mm <sup>2</sup> )	( N/mm <sup>2</sup> )	
CFS	2.4	560.5	636.7	182000.0	1.1
Wire Mesh	Ø6	712.6	725.3	149000.0	1.0
	Ø12	656.6	746.6	213333.3	1.1
Reinforcement	Ø16	525.0	599.0	218333.3	1.1
	Ø20	574.3	666.3	214333.3	1.1

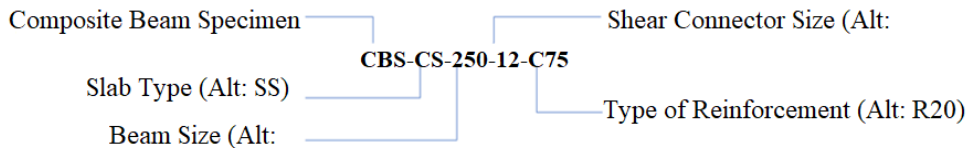


**Figure 11.** Specimen labelling

## 2.8 Material Properties

Compressive strength tests on standard concrete cubes (150 mm × 150 mm × 150 mm) and cylinders (150 mm × 300 mm) were performed to determine the concrete's modulus of elasticity and compressive strength at this angle. After being made and let to cure for 28 days, the cubes and cylinders were then put through their paces in terms of failure testing. We followed the instructions in BS EN 12504-1 when we conducted the compression tests. The compressive strengths obtained from the concrete cubes ( $Z - cb$ ) and the concrete cylinders ( $b - cd$ ) are listed in Table 2. The angle's concrete's modulus of elasticity,  $E - c$ , is listed in Table 2 for your reference. The material properties of the composite materials (reinforcement mesh, shear connectors, and CFS channel components) used in the design of the suggested composite specimen have been confirmed. Following testing in compliance with BS EN 10002-1, coupons were efficiently cut from the longitudinal and transverse orientations of the CFS channel sections using efficient computer simulations. In Table 3, you can see the yield strength ( $f - y$ ), ultimate strength ( $f - u$ ), and modulus of elasticity ( $E - y$ ) of the steel parts (Figure 12).



**Figure 12.** Welding without ceramic ferrule

### 3 Experimental Results

#### 3.1 General Observations

##### 3.1.1 AISC 2005, EC-4, ACI 318-08, and PCI 6th edition

The current formula for the nominal shear strength of a steel anchor (other than in composite beams) in AISC ( $0.5A_s\sqrt{f'_c}E_c < A_sF_u$ ) and EC-4 ( $C_v0.5A_s\sqrt{f'_c}E_{cm}$ ) was computed for each of the 391 tests (using the minimum value of the steel and concrete failure modes) using efficient computer simulation (Figure 13). In these formulas, measured values of  $E_c$  are used or not,  $E_c$  is calculated per ACI 318-08 by the measured properties of the concrete strength.  $E_{cm}$  is computed per [19, 20] through the measured properties of concrete strength (Figure 14). Measured  $F_u$  values were not provided by the authors in a very small number of cases (specified (nominal) values of  $F_u$  was used here).

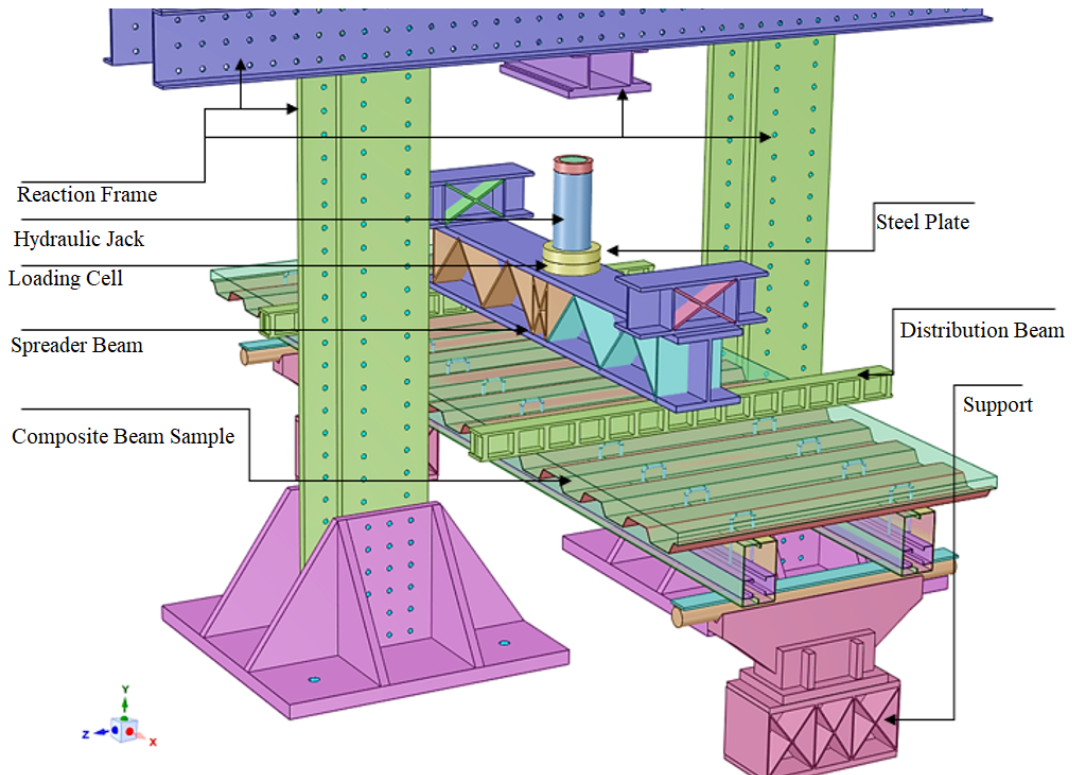


**Figure 13.** Test set up

#### 3.2 Effect of Different Parameters on Ultimate Load and Bending Resistance

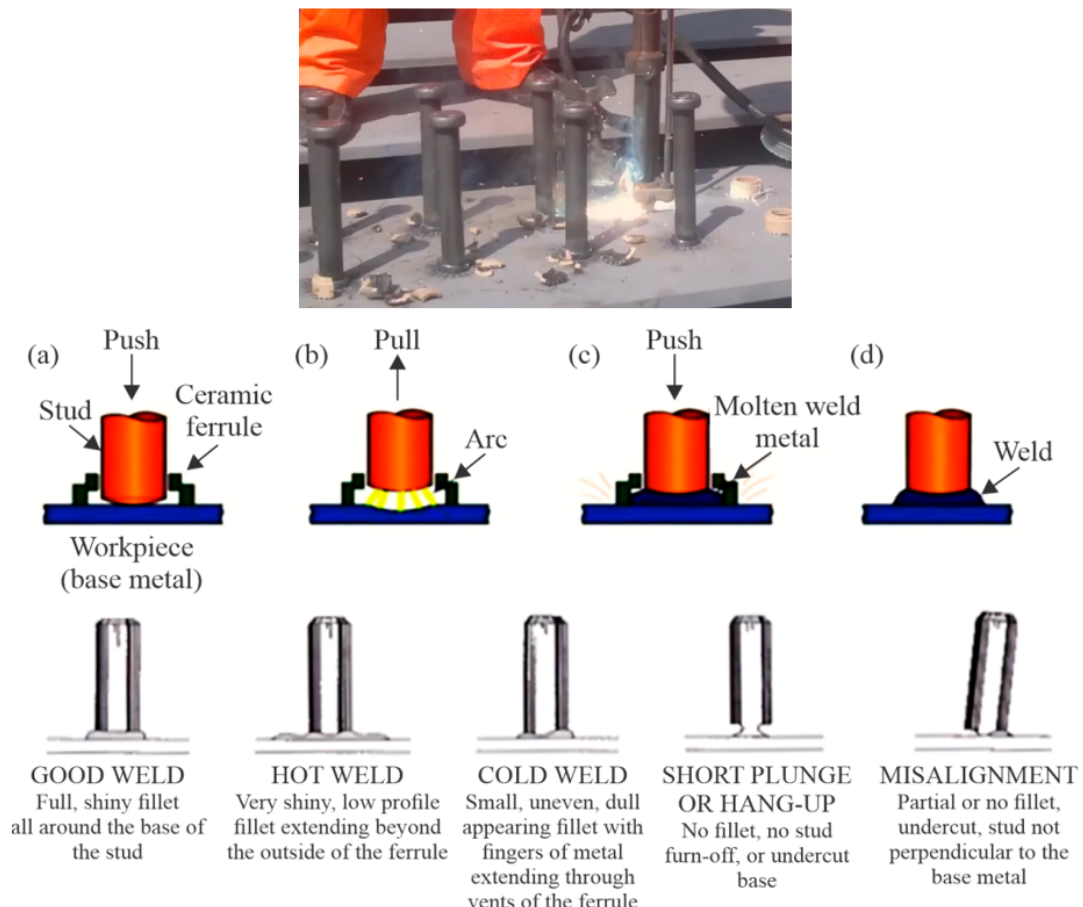
##### 3.2.1 Depth of CFS composite built-up box beams

Figure 15 illustrates that an increase in beam depth correlates with enhanced stiffness and reduced deflection across all test specimens. The comparison of test specimens (CBS1 vs CBS2, CBS3 versus CBS4, and CBS6 versus

CBS7) indicates that an increase in beam depth has led to a reduction in beam deflection. This activity was closely associated with the rigidity of the composite beam. Figure 15 illustrates that the composite specimens with a beam depth of 150 mm exhibited greater flexibility and reduced stiffness. The moment of inertia for 150 mm deep beams decreased by 80.3% relative to that of 250 mm deep beams. Conversely, the bending resistance of composite systems using 150 mm deep beams decreased by 55.9% in comparison to that of systems utilising 250 mm deep beams.



**Figure 14.** Observations from specimens



**Figure 15.** Drawn-Arc angle welding

### 3.2.2 Type of slab

The kind of steel decking may substantially influence the bending resistance of the composite system, particularly with shallow beams. Two distinct kinds of slabs were used in the tests: profiled deck slabs and solid deck slabs. The steel decking decreased concrete use by 25% for both the 250 mm and 150 mm deep beams. Nonetheless, the impact varies across the specified beam depths (comparing CBS1 with CBS6 and CBS2 with CBS7). The use of a contoured deck slab with a beam depth of 250 mm resulted in an 18.7% reduction in section resistance load compared to the section resistance of the solid deck slab (Figure 16). Conversely, with the contoured deck slab with a beam depth of 150 mm, the section resistance load decreased by 34.1% relative to the section resistance of the solid deck slab. This

behaviour may result from increased resistance in the compression zone when the slab transitioned from profiled decking to solid slab.

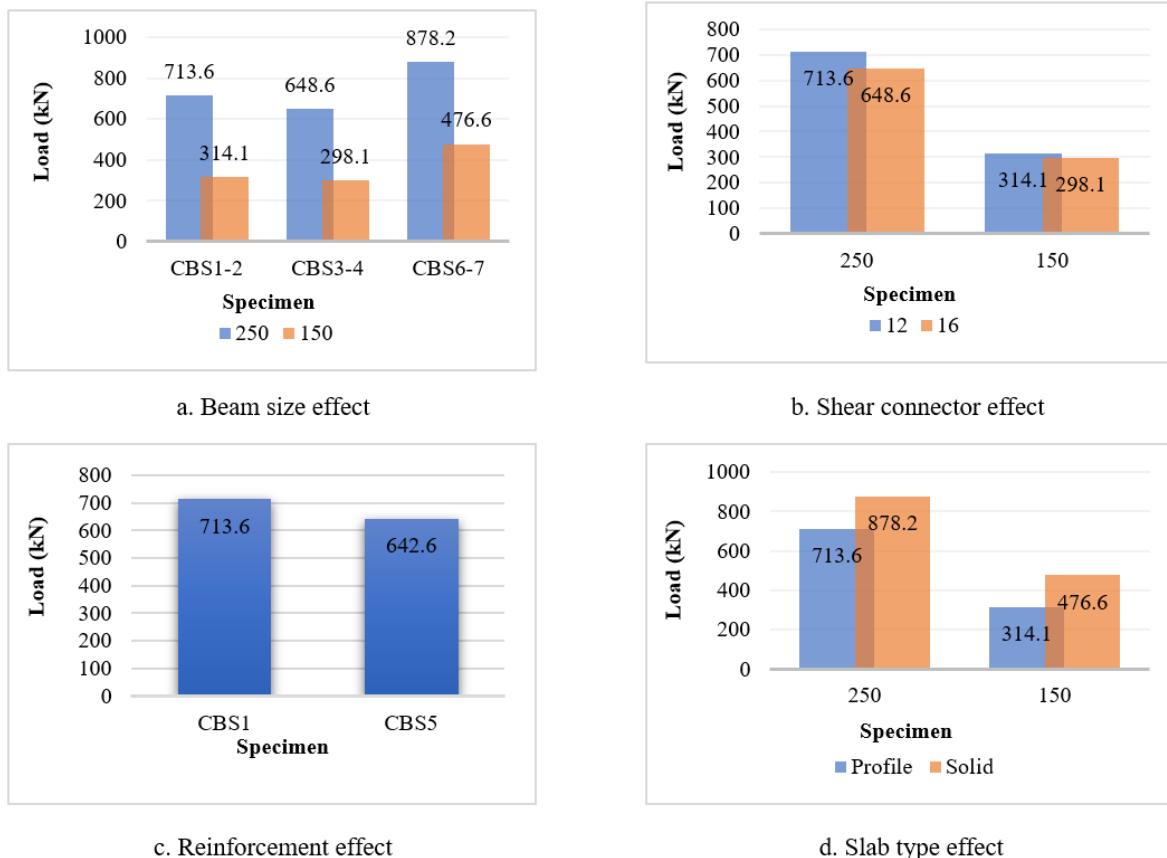


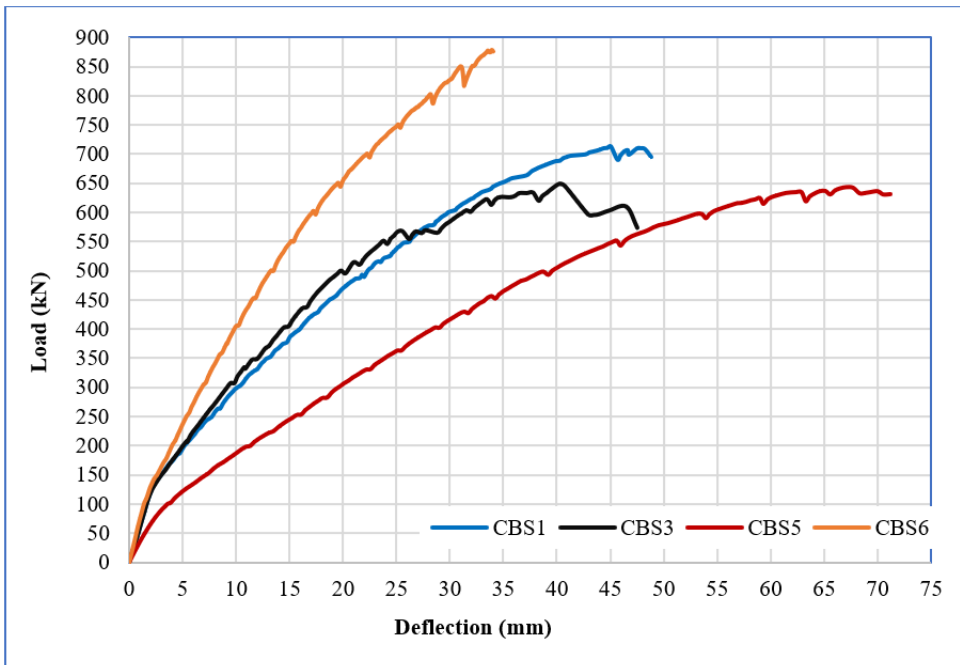
**Figure 16.** Effect of different parameters on ultimate load

### 3.3 Load-Deflection Curves

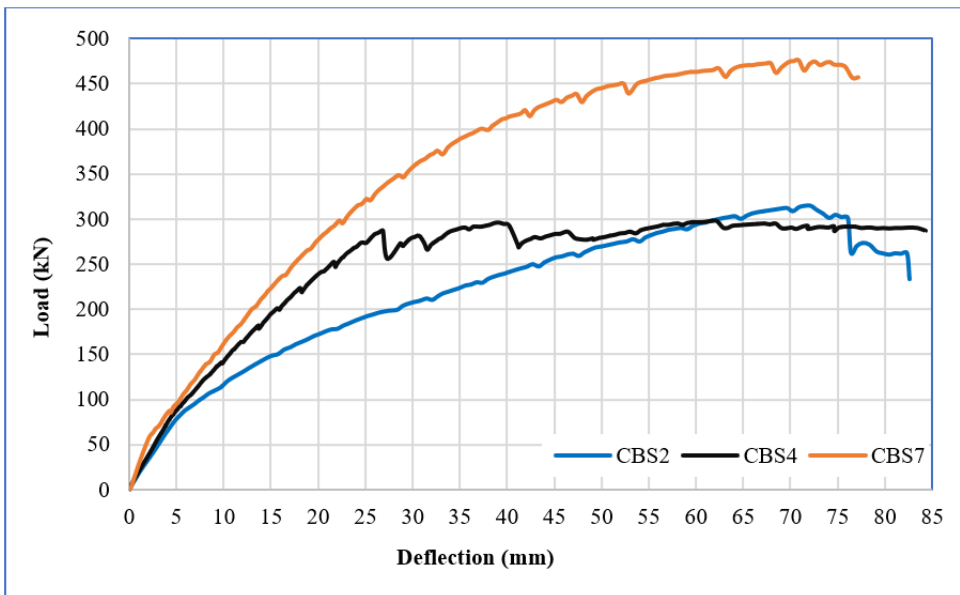
The load-deflection behaviour was documented for all test specimens and shown in Figure 17. The load-deflection curves exhibited linearity during the early loading phase but transitioned to non-linearity after loading beyond the elastic limit. Table 4 highlights the experimental test findings derived from the load-deflection curves, including ultimate load, corresponding mid-span deflections  $\delta_u$ , ultimate bending resistance moment, and failure modes, using efficient computer modeling. All specimens exhibited transverse and longitudinal fissures on the upper surface of the slab. The CFS composite built-up box section beams exhibited local buckling but sustained loads until yielding or, in some instances, rupture occurred. Among all examples, specimen CBS6 had the greatest ultimate bending resistance, suggesting that increasing the depth of the concrete slab and transitioning from profiled decking to a solid slab enhances the bending resistance of the proposed composite beam. Furthermore, it was determined that the ultimate bending resistance of Specimen CBS4 was the lowest. This discovery indicates that the beam's depth substantially influences the composite beam's bending resistance.

**Table 4.** Experimental test results

Specimen ID	$P_u$ kN	$\delta_u$ mm	$M_u$ kNm
CBS1	713.6	48.8	356.8
CBS2	314.1	82.6	157.0
CBS3	648.6	47.5	324.3
CBS4	298.1	84.3	149.0
CBS5	642.6	71.1	321.3
CBS6	878.2	34.0	439.1
CBS7	476.6	77.2	238.3



(a) 250 mm deep beams



(b) 150 mm deep beams

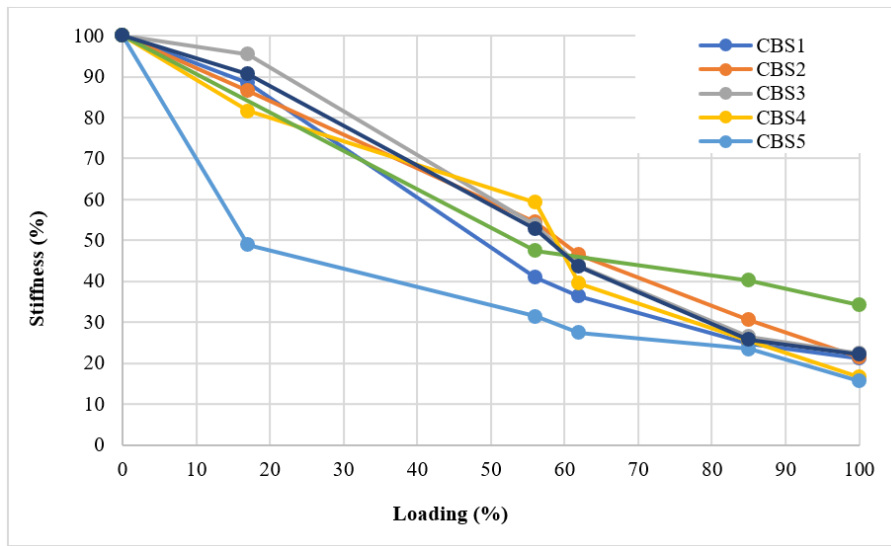
**Figure 17.** Applied loads versus mid-span deflection curves

The composite system, with solid slabs, had higher ultimate stiffnesses by around 38.0-43.2% when compared to the composite specimens with profiled deck slabs (Figure 18).

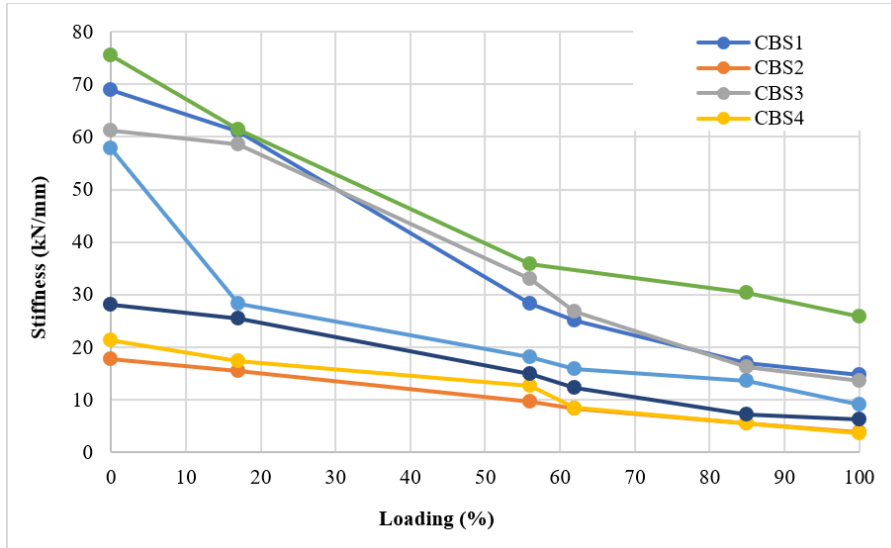
Based on the load-deflection curves of the experimental results shown in Figure 18 and Table 5. The composite beam resistance  $N_{pl,a}$ , slab resistance  $N_{c,f}$ , shear connectors resistance  $R_q$ , the degree of shear connection  $k$ , the full composite action of the system  $M_{pl,Rd}$ , and the partial composite action of the system, which is the predicted ultimate bending resistance of each specimen, based on Eurocode EC4, is denoted as  $M_{EC4}$ . The calculated bending resistance for all test specimens are listed in Table 5, where the ratios of calculated test values are given for comparison purposes. As indicated, the average ratio of  $M_u/M_{EC4}$  is 0.75, being a 24.7% overestimate of the test results, therefore, design improvements are needed for such a composite system to better predict the bending resistance (Figure 19).

**Table 5.** Comparison of bending resistances from the tests and Eurocode EC4

Specimen ID	Experimental Results		Predicted Bending Resistance Based on Eurocode EC4					
	$M_u$ (kNm)	$N_{pl,a}$ (kN)	$N_{c,f}$ (kN)	$R_q$ (kN)	k	$M_{pl,Rd}$ (kNm)	$M_{EC4}$ (kNm)	$M_u/M_{EC4}$ (kNm)
CBS1	356.80	1384.58	1080.82	1319.76	1.00	411.94	411.94	0.86
CBS2	157.05	888.33	1080.82	1319.76	1.00	270.14	270.14	0.58
CBS3	324.30	1384.58	1080.82	1462.76	1.00	411.94	411.94	0.78
CBS4	149.05	888.33	1080.82	1462.76	1.00	270.14	270.14	0.55
CBS5	321.30	1366.45	1080.82	1319.76	1.00	412.84	412.84	0.77
CBS6	439.10	1384.58	2161.64	1319.76	0.95	476.40	460.72	0.95
CBS7	238.30	888.33	1678.75	1319.76	1.00	317.60	317.6	0.75
Mean	283.70						364.61	0.75
Percentage Error %								24.7



(a) Flexural stiffness ratio-loading relationship



(b) Flexural stiffness-loading relationship

**Figure 18.** Flexural stiffness behavior of the test specimens

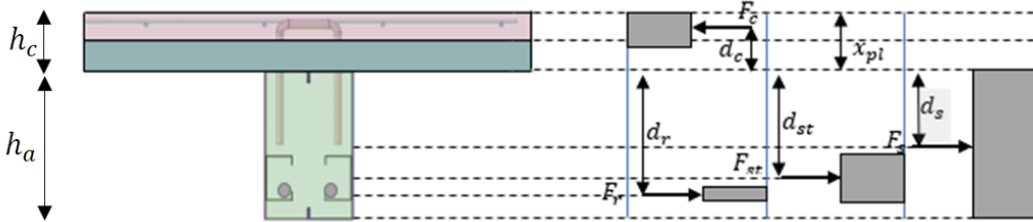


**Figure 19.** Calculation model for the bending resistance

The design value of the bending resistance of the beam is:

$$N_{pl,a} = A_s \cdot f_{ys} + A_r \cdot f_{yr} + A_{st} \cdot f_{yst} \quad (11)$$

or

$$N_{pl,a} = F_s + F_r + F_{st} \quad (12)$$

The resistance of the effective area of the concrete flange acting compositely with the economic composite beam is:

$$N_{c,f} = A_c \cdot 0.85 \cdot f_{cd} \quad (13)$$

The neutral axis lies at distance  $x_{pl}$  below the top face of the concrete slab and can be calculated by using Eq. (14):

$$x_{pl} = \frac{N_{pl,a}}{N_{c,f}} \cdot h_c \quad (14)$$

The bending resistance moment with the full shear connection  $M_{pl,Rd}$  may be determined from Eq. (15) as given below:

$$M_{pl,Rd} = N \cdot \left( \frac{h_a}{2} + h_c - \frac{x_{pl}}{2} \right) \quad (15)$$

The bending resistance moment of a composite beam with the partial shear connection is obtained as follows (Table 6):

$$M_{Rd} = M_{a,Rd} + \frac{R_q}{N} \cdot (M_{pl,Rd} - M_{a,Rd}) \quad (16)$$

**Table 6.** Comparison of bending resistances from the tests and improved design rules

Specimen ID	Experimental Results			EC4		Improved Design Rules			
	$M_u$ (kNm)	$k$	$M_{pl,Rd}$ (kNm)	$M_{EC4}$ (kNm)	$M_u/M_{EC4}$	$k_m$	$M_{pl,Rd}$ (kNm)	$M_{Rd}$ (kNm)	$M_u/M_{Rd}$
CBS1	356.80	1.00	411.94	411.94	0.86	0.78	411.94	351.58	1.01
CBS2	157.05	1.00	270.14	270.14	0.58	0.51	270.14	172.54	0.91
CBS3	324.30	1.00	411.94	411.94	0.78	0.65	411.94	315.44	1.03
CBS4	149.05	1.00	270.14	270.14	0.55	0.35	270.14	140.20	1.06
CBS5	321.30	1.00	412.84	412.84	0.77	0.78	412.84	352.20	0.91
CBS6	439.10	0.95	476.40	460.72	0.95	0.95	476.40	460.72	0.95
CBS7	238.30	1.00	317.60	317.6	0.75	0.51	317.60	196.96	1.20
Mean	283.70				0.75				1.01
Percentage Error %					24.7				7.4
COV					0.19				0.10
Standard Deviation					0.13				0.09

## 4 Conclusions

Limited state formulae for heading angle anchors in composite structures were evaluated according to AISC and EC-4 criteria; 391 monotonic and cyclic tests were compared, and ACI 318-08 was compared to the Building Code and the 6th Edition PIC manual. We provide new equations for the prediction of concrete failures and use a comprehensive experimental dataset to assess the performance of existing formulae for the prediction of steel failures. Using efficient computer modeling, the test results have been disaggregated to highlight failures in the concrete, mixed failure tests, and the steel shank or weld. Composite beam-columns, composite wall system boundary components, related composite construction measures, concrete-encased and concrete-filled beams, composite connections, and composite column base conditions are the main points of this examination. When it comes to composite construction, pryout failure is more common than breakout failure, according to ACI 318-08. This is because the majority of composite structures do not have enough failure planes for front and side breakouts. Concrete breakout intensity is not considered a regulatory limiting requirement, according to this research. If a resistance factor is applied to offer an adequate level of reliability, ( $\text{AsFu}$ ) may accurately predict the mechanism of steel failure in heading angle anchors. Around 4 is the dependability index  $\beta$  that results from a resistance factor of 0.65. If  $\text{AsFu}$  is reduced by 0.65, then a resistance factor of 1.0 may be applied. When resistance is taken into account, EC-4 (2004) usually produces conservative results for concrete and steel failures. An alternate method to the current forecasts for concrete failures in AISCC 2005 is proposed, which involves a series of formulas for pryout failure estimates. When controlling the concrete failure strength, it is appropriate to use formulae based on the sorts of parameters.

## Data Availability

Not applicable.

## Conflicts of Interest

The authors declare no conflict of interest.

## References

- [1] T. T. Soong and G. F. Dargush, *Passive Energy Dissipation Systems in Structural Engineering*. John Wiley & Sons, 1997.
- [2] T. T. Soong and B. F. Spencer Jr, “Supplemental energy dissipation: State-of-the-art and state-of-the-practice,” *Eng. Struct.*, vol. 24, no. 3, pp. 243–259, 2002. [https://doi.org/10.1016/S0141-0296\(01\)00092-X](https://doi.org/10.1016/S0141-0296(01)00092-X)
- [3] R. Nian, B. He, B. Zheng, M. Van Heeswijk, Q. Yu, Y. Miche, and A. Lendasse, “Extreme learning machine towards dynamic model hypothesis in fish ethology research,” *Neurocomputing*, vol. 128, pp. 273–284, 2014. <https://doi.org/10.1016/j.neucom.2013.03.054>
- [4] S. S. Abdullah, M. A. Malek, N. S. Abdullah, O. Kisi, and K. S. Yap, “Extreme learning machines: A new approach for prediction of reference evapotranspiration,” *J. Hydrol.*, vol. 527, pp. 184–195, 2015. <https://doi.org/10.1016/j.jhydrol.2015.04.073>
- [5] A. S. U. S. Manual, *Version 6.10. ABAQUS*. Inc, Rhode Island, 2010.
- [6] G. B. Huang, Q. Y. Zhu, and C. K. Siew, “Real-time learning capability of neural networks,” *IEEE Trans. Neural Netw.*, vol. 17, no. 4, pp. 863–878, 2006. <https://doi.org/10.1109/TNN.2006.875974>
- [7] D. Wang and G. B. Huang, “Protein sequence classification using extreme learning machine,” in *2005 IEEE International Joint Conference on Neural Networks, Montreal, Que*, 2005, pp. 1406–1411. <http://doi.org/10.1109/IJCNN.2005.1556080>
- [8] K. C. Chang, M. L. Lai, T. T. Soong, D. S. Hao, and Y. C. Yeh, *Seismic Behavior and Design Guidelines for Steel Frame Structures with Added Viscoelastic Dampers*. Buffalo, NY, USA: National Center for Earthquake Engineering Research, 1993.
- [9] K. C. Chang, T. T. Soong, M. L. Lai, and E. J. Nielsen, “Viscoelastic dampers as energy dissipation devices for seismic applications,” *Earthq. Spectra*, vol. 9, no. 3, pp. 371–387, 1993. <https://doi.org/10.1193/1.1585721>
- [10] K. Kasai, “Viscoelastic damper hysteresis model: Theory, experiment, and application,” in *ATC17-1 Seminar, Applied Technology Council*, 1993, pp. 521–532.
- [11] S. H. Lee, D. I. Son, J. Kim, and K. W. Min, “Optimal design of viscoelastic dampers using eigenvalue assignment,” *Earthq. Eng. Struct. Dyn.*, vol. 33, no. 4, pp. 521–542, 2004. <https://doi.org/10.1002/eqe.364>
- [12] D. De Domenico and I. Hajirasouliha, “Multi-level performance-based design optimisation of steel frames with nonlinear viscous dampers,” *Bull. Earthquake Eng.*, vol. 19, no. 12, pp. 5015–5049, 2021. <https://doi.org/10.1007/s10518-021-01152-7>
- [13] Y. Zhou, M. Aguaguiña, D. E. Beskos, and S. Gong, “A displacement-based seismic design method for building structures with nonlinear viscoelastic dampers,” *Bull. Earthquake Eng.*, vol. 19, no. 9, pp. 4981–5014, 2021. <https://doi.org/10.1007/s10518-021-01135-8>

- [14] J. Ricles, R. Sause, and B. Dong, “Enhanced seismic efficiency and resiliency of steel-frame buildings using viscous-dampers,” in *International Conference on the Behaviour of Steel Structures in Seismic Areas*, 2024, pp. 230–242. [http://doi.org/10.1007/978-3-031-62888-7\\_21](http://doi.org/10.1007/978-3-031-62888-7_21)
- [15] F. S. Dizaji and M. S. Dizaji, “A novel smart memory alloy re-centering damper for passive protection of structures subjected to seismic excitations using high-performance nitihfpd material,” *arXiv preprint*, 2021. <https://doi.org/10.48550/arXiv.2105.04081>
- [16] N. Pollini, “Fail-safe optimization of viscous dampers for seismic retrofitting,” *Earthq. Eng. Struct. Dyn.*, vol. 49, no. 15, pp. 1599–1618, 2020. <https://doi.org/10.1002/eqe.3319>
- [17] A. Shirkhani, B. F. Azar, and M. C. Basim, “Evaluation of efficiency index of friction energy dissipation devices using endurance time method,” *Numer. Methods Civ. Eng.*, vol. 5, no. 2, pp. 12–20, 2020. <https://doi.org/10.52547/nmce.5.2.12>
- [18] A. A. Alhasan, M. Vafaei, and S. C. Alih, “Viscoelastic dampers for protection of structures against seismic actions,” *Innov. Infrastruct. Solut.*, vol. 7, no. 3, p. 743, 2022. <http://doi.org/10.1007/s41062-022-00905-w>
- [19] N. Pollini, O. Lavan, and O. Amir, “Towards realistic minimum-cost optimization of viscous fluid dampers for seismic retrofitting,” *Bull. Earthq. Eng.*, vol. 14, no. 3, pp. 1013–1038, 2016.
- [20] S. Kitayama and M. C. Constantinou, “Fluidic self-centering devices as elements of seismically resistant structures: Description, testing, modeling, and model validation,” *J. Struct. Eng.*, vol. 143, no. 7, p. 04017050, 2017. [http://doi.org/10.1061/\(ASCE\)ST.1943-541X.0001787](http://doi.org/10.1061/(ASCE)ST.1943-541X.0001787)

## Nomenclature

$L$	Beam length
$L_0$	Effective beam span
$B$	Concrete slab width
$f_{cu}$	Cube compressive strength of concrete
$f_{vr}$	The yield strength of reinforcement
$f_{vst}$	The yield strength of stiffener
$f_{cd}$	Cylinder strength of the concrete
$f_s$	The resultant force of CFS beam
$E_c$	Modulus of elasticity of concrete
$f_u$	Ultimate tensile strength of steel
$E_s$	The elastic modulus of steel
$h_p$	The depth of the steel profile
$h_c$	The depth of the concrete slab
$h_a$	The depth of the CFS beam
$h_0$	The effective depth of the CFS beam
$\rho$	Reinforcement ratio
$P_u$	Ultimate load
$\delta_u$	Ultimate deflection
$M_u$	Ultimate moment experimentally
$A_s$	Area of CFS beam
$A_r$	Area of reinforcement
$A_{st}$	Area of stiffener
$A_c$	Area of the concrete slab
$f_{vs}$	The yield strength of CFS beam
$F_r$	The resultant force of reinforcement
$F_{st}$	The resultant force of stiffener
$N_{pl,a}$	Tensile resistance of steel
$N_{c,f}$	Compressive resistance of the concrete flange
$x_{pl}$	Neutral axis
$M_{pl,Rd}$	Bending resistance moment with full shear connection
$N$	The lesser of $N_{pl,a}$ and $N_{c,f}$
$R_q$	The resistance of shear connectors
$k$	Degree of shear connection
$k_m$	Modified degree of shear connection
$M_{a,Rd}$	Bending resistance moment of the composite beam
$M_{EC4}$	Bending resistance moment of the composite beam allowing for partial shear connection using EC4
$M_{Rd}$	Bending resistance moment of the composite beam allowing for partial shear connection using improved approach